Design Optimization of a Robust Sleeve Antenna for Hepatic Microwave Ablation

Punit Prakash[1], Geng Deng[2], Mark C Converse[3], John G Webster[1], David M Mahvi[3] and Michael C Ferris[4]

[1]Department of Biomedical Engineering, University of Wisconsin, Madison, WI 53706, USA
[2]Department of Mathematics, University of Wisconsin, Madison, WI 53706, USA
[3]Department of Surgery, University of Wisconsin, Madison, WI 53792, USA
[4]Computer Sciences Department, University of Wisconsin, Madison, WI 53706, USA

E-mail: pprakash@cae.wisc.edu, deng@math.wisc.edu and webster@engr.wisc.edu

Abstract. We describe the application of a Bayesian variable-number sample-path (VNSP) optimization algorithm to yield a robust design for a floating sleeve antenna for hepatic microwave ablation. Finite element models are used to generate the electromagnetic (EM) field distribution in liver given a particular design. Dielectric properties of the tissue are assumed to vary within $\pm 10\%$ of average properties to simulate the variation among individuals. The Bayesian VNSP algorithm yields an optimal design that is a 27.3% improvement over the original design and is more robust in terms of lesion size, shape and efficiency. Moreover, the Bayesian VNSP algorithm finds an optimal solution saving 41% simulation of the evaluations compared to the standard sample-path optimization method.

Submitted to: *Phys. Med. Biol.*

1. Introduction

Microwave ablation for the treatment of hepatic and metastatic tumours is a promising alternative when surgical resection – the gold standard – is not practical. In this procedure, a thin, coaxial antenna (probe) is inserted into the tumour (either percutaneously or during open surgery) and microwaves are radiated into the tissue. The alternating fields cause rapid rotation of the polar water molecules resulting in heating of tissue and ultimately leading to cell death. This cell death is a function of both temperature and time, where higher temperatures lead to cell death in a shorter period of time. Since studies indicate that coagulated necrosis of tissue can be achieved within a few seconds at 60 °C, a common metric to predict cell death and ultimately lesion size is the 60 °C contour. Since this 60 °C metric is valid for both cancerous and normal tissue, design of the antenna radiation pattern is critical to achieve a heating pattern affecting only cancerous tissue. To meet these design needs, several types of coaxial antennas have been have been proposed and optimized for this for this application and are reviewed in Bertram et al (2006).

When optimizing a design or studying performance, most studies use average dielectric properties for liver tissue that have been measured previously and are readily available in the literature (Gabriel et al 1996). However, due to the natural variation in tissue among individuals, measured dielectric properties of healthy and tumourous liver tissue may differ by as much as ±10% from the average value (Stauffer et al 2003). This variation means that a given patient's tissue may not have the same dielectric properties as those used in the design of an antenna, leading to suboptimal performance. Therefore it is important to ensure that antennas to be used for hepatic microwave ablation are robust, i.e., relatively insensitive to changes in physical properties of the tissue.

We present a method for optimizing a coaxial antenna for microwave ablation of hepatic and metastatic tumours that takes into account the variability in liver dielectric properties among individuals. This adds additional complexity to the optimization problem since the performance of a particular design is now a function of its dimensions (the design variables), as well as some unknown variation in tissue properties. To design an antenna with robust performance, we apply a sample-path optimization method (or sample average approximation method) (Kleywegt et al 2001, Plambeck et al 1996, Robinson 1996), which averages repeated evaluations of a design to reduce variation. Since we use a common random number (CRN), it can be shown that under mild conditions the limit points of solutions of the sampled problem lie almost surely in the solution set of the underlying problem. The sample-path method has been applied to a number of optimization problems including option pricing (Gürkan et al 1996), scheduling (Plambeck et al 1993), and network design (Gürkan et al 1999). In the optimization process, the task of determining the number of replicated samples is handled by the Bayesian Variable-Number Sample-Path (VNSP) scheme (Deng and Ferris 2007). Compared to the standard sample-path method with a fixed number of samples, the VNSP scheme uses fewer objective function evaluations and

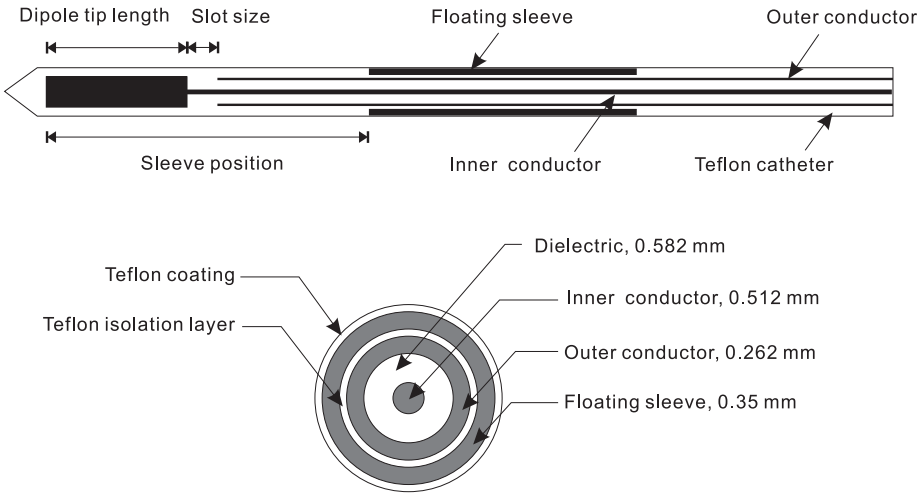

Figure 1. Structure of the floating sleeve antenna. Wall thicknesses of fixed dimensions are labelled in the figure.

is therefore more economical since these are computationally expensive to evaluate. We embed the VNSP scheme in Powell's UOBYQA (Unconstrained Optimization BY Quadratic Approximation) optimization method (Powell 2002), an efficient derivative-free algorithm.

To perform this optimization we rely upon computer models. Computer models are a widely used tool in the design of antennas for microwave ablation as they provide a quick, convenient and accurate method of estimating antenna performance. Given the physical properties of liver tissue and tumour, such models can be used to predict the EM field distribution and resistive heating in tissue due to a particular antenna design. A quantitative assessment of a particular antenna design may then be obtained by extracting appropriate metrics from solutions provided by the computer model. Suitable metrics may be the efficiency of the antenna (fraction of the power supplied that is deposited into the liver), size and shape of the predicted lesion compared to the tumour, and diameter of the antenna. An optimization problem may then be formulated where the design variables are the dimensions of the antenna, and the objective function is obtained by combining the metrics in some fashion (Iskander and Tumeh 1989). The floating sleeve antenna presented in Yang et al (2006) was chosen to be optimized in this study due to its ability to create large, constrained lesions. A schematic of the antenna is shown in figure 1. We have identified dimensions of this antenna that may be optimized to yield desirable lesion size, shape and efficiency, and we minimize the overall diameter of the probe.

The rest of this paper is organized as follows. The next section describes the computer model and formulation of the optimization problem at hand. Section 3 briefly explains the UOBYQA optimization algorithm with the integration of the VNSP scheme. Section 4 presents and discusses the results of applying this procedure to the optimization problem. Finally, a conclusion and discussion of future work is presented

Table 1. Design metrics in the sleeve antenna.

Parameter	Range of values
Length of dipole tip	1 – 60 mm
Slot size	1 – 50 mm
Sleeve position	1 – 60 mm
Thickness of Teflon coating	0.1 – 1 mm
Thickness of Teflon isolation layer	0.1 – 1 mm
Length of sleeve	5 – 50 mm

in section 5.

2. Methods

2.1. Floating sleeve antenna

Yang et al (2006) presented a floating sleeve antenna consisting of a coaxial dipole antenna with a floating sleeve used to constrain power deposition to the distal end. The structure of the antenna is shown in figure 1. For a particular operating frequency (usually 915 MHz or 2.45 GHz), dimensions of the antenna that affect the radiation pattern and efficiency of the antenna are: (a) length of the dipole tip, (b) slot size, (c) sleeve position, (d) thickness of Teflon isolation layer, (e) thickness of Teflon coating and (f) sleeve length. Throughout this paper, an individual design, $x \in \mathbb{R}^6$, may be expressed as the vector of the design variables (a)–(f), in mm. As explained in Yang et al (2006), the floating sleeve is effective in constraining the lesion longitudinally when it is approximately a half wavelength long. Note that this is not half the wavelength of a plane wave propagating through either liver or the Teflon of the catheter. Rather, this is half a wavelength in the layered Teflon/liver medium (outside the metal sleeve) whose effective properties are somewhere between those of liver and Teflon and is a function of the Teflon thickness. Therefore since we are varying the thickness of the Teflon layers we expect the optimal sleeve length to change as well. Table 1 shows the range over which of the dimensions (a)–(f) were varied.

2.2. Finite element model of coaxial sleeve antenna

For this study we used the commercial *finite element* (FE) package, COMSOL Multiphysics v3.2 (COMSOL Inc. Burlington, MA) to simulate antenna performance and determine the objective function for a given antenna design. This software allows us to specify the geometry of an antenna design and then solves Maxwell's equations in the surrounding tissue. We coupled this software with MATLAB, to perform the optimization of the antenna.

The model involves the antenna inserted into an infinitely large piece of liver. Dimensions of the antenna as well as design variables are illustrated in figure 1.

Input power was set to 120 W at an operating frequency of 2.45 GHz. Due to the cylindrical symmetry of the geometry, we were able to reduce computational burden by implementing an axially symmetric model. A steady state nonlinear solver was used to compute the resistive heating ($Q(\boldsymbol{r})$) which is proportional to the square of the local electric field. Computation time for each simulation was approximately 11 s on a computer with a 3 GHz Intel P4 processor and 1 GB memory.

Typically, constant values of dielectric properties are assumed when designing an antenna. Often these properties are obtained from average values reported in the literature for healthy human liver (Duck 1990, Gabriel et al 1996, Stauffer et al 2003). However there is a natural variation in tissue among individuals. Stauffer et al (2003) have measured dielectric properties of healthy and tumourous ex-vivo human liver at room temperature in the 0.3–3 GHz range. Their results show standard deviations of $\pm 10\%$ in samples taken from different individuals. Also, it is expected that the dielectric properties of this tissue will vary during the course of ablation as tissue water content and temperature change from their steady state values. As such, it is important to ensure that antennas used for microwave ablation are robust, i.e., relatively insensitive to changes in the physical properties of tissue. In this study, we used average values of dielectric constant (43.03) and conductivity (1.69), as in Yang et al (2006) and assumed these dielectric properties vary randomly as a Gaussian distribution with standard deviation $\pm 10\%$ about this mean. Thus, the dielectric constant and conductivity may be expressed as $\mathcal{N}(43.03, 4.303^2)$ and $\mathcal{N}(1.69, 0.169^2)$. While we do not account for changes in dielectric properties during the course of ablation, because the antenna is more robust to variations in tissue properties, it should lead to a better performance with respect to dielectric property changes during the course of ablation. Moreover, it may be possible to utilize this noisy optimization algorithm to take into account these changes in future studies.

The resistive heating ($Q(\boldsymbol{r})$) profiles calculated by the FE model are used as input to a thermal model which predicts temperature profiles from which an estimate of lesion size is obtained. For computational efficiency, we have chosen to use a simple thermal model

$$Q(\boldsymbol{r}) = \rho c \frac{\mathrm{d}T(\boldsymbol{r})}{\mathrm{d}t}, \tag{1}$$

where c [J/(kg·K)] and ρ [kg/m^3] are the specific heat capacity and density of liver tissue, respectively, and dT/dt [K/s] is the change in local temperature with time. Here, for computational efficiency, we have ignored thermal conductivity and the (cooling) effects of blood perfusion. The lesion size and shape metrics are calculated using the 60 °C contour after 180 s with an input power of 120 W.

2.3. Objective metrics for assessing antenna performance

In this study we are optimizing for lesion size and shape, antenna efficiency and antenna size. In practice, design variables may be selected to fit the heating pattern of an antenna

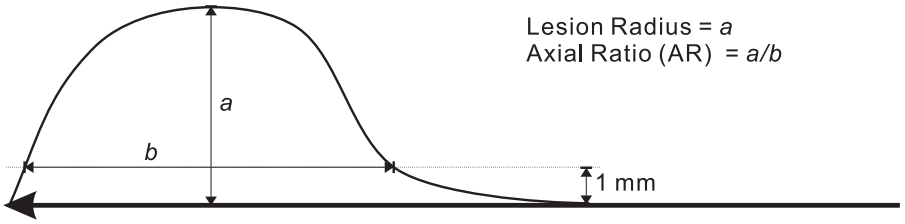

Figure 2. Objective metrics for assessing size and shape of a $Q(\boldsymbol{r})$ profile

Table 2. Objective metrics in the sleeve antenna design.

Metric	Measure of	Goal
Lesion radius	Size of lesion in radial direction	Maximize
Axial ratio	Proximity of lesion shape to a sphere	Fit to 0.5 (see figure 2)
S_{11}	Efficiency of antenna	Minimize (or maximize $\|S_{11}\|$)
Probe radius	Radial size	Minimize

to the tumour at hand. Since most tumours are spherical in shape (Yang et al 2006), our goal in this study was to optimize an antenna to yield the lesion with largest radius and having a shape that is as close to a sphere as possible. We identified two metrics to assess the size and shape of the lesion: lesion radius and axial ratio. These metrics are illustrated for an example $Q(\boldsymbol{r})$ profile in figure 2. Note that an axial ratio (as annotated in figure 2) of 0.5 would yield a spherical lesion shape. The efficiency of an antenna may be measured by computing the reflection coefficient ($S_{11}dB$) – the ratio of power reflected to power input. The more negative the S_{11}, the more power is coupled into the liver. Reflected power was calculated from the FE model by sampling the net time-averaged power flow at the antenna feedpoint and subtracting from the input power (120 W). Finally, the antenna being optimized may be used in a minimally invasive procedure (i.e., percutaneously); thus, it is desirable to yield a design with the smallest radius. These objective metrics are summarized in table 2.

We employ an algorithm that only handles a single objective function and so the above four objectives need to be combined. A simple way to do this is to assign weights to each metric, based on their relative importance, and then sum up the weighted objectives. Since the range over which these objectives vary is not the same, we normalized each objective by their largest possible value so that the weighted sum is not skewed by the scale of each individual metric. Each metric was deemed to be equally important and so identical weights of 0.25 were assigned to each normalized objective. The optimization problem thus formulated is written as:

$$\min_{x\in\mathbb{R}^n} F(x) := \mathbb{E}_\omega\left[f(x,\omega)\right] \tag{2}$$
$$= \mathbb{E}_\omega\left[-p_1\frac{\text{Lesion}(\omega)}{H_1} + p_2\frac{|\text{AR}(\omega)-0.5|}{H_2} + p_3\frac{S_{11}(\omega)}{H_3} + p_4\frac{\text{Probe}(\omega)}{H_4}\right],$$

where the weights $p_1 = p_2 = p_3 = p_4 = 0.25$ and H_i represent normalization values. The function $f(x,\omega)$ is often called the sample response function. The optimization formulation (2) aims to maximize the expected performance among different individuals, whose specific physical parameters ω are extracted from predefined distributions. (In our case ω indicates the dielectric properties.) Besides (2), other robust formulations such as $\min_{x\in\mathbb{R}^n}\max_{i=1}^N f(x,\omega_i)$ and $\min_{x\in\mathbb{R}^n}\min_{i=1}^N f(x,\omega_i)$ are possible, but these are not discussed here.

3. Bayesian Variable-Number Sample-Path (VNSP) Optimization

3.1. Introduction to VNSP optimization

Consider the generalized formulation for the robust antenna design problem

$$\min_{x\in\mathbb{R}^n} F(x) = \mathbb{E}_\omega[f(x,\omega)]. \tag{3}$$

The sample-path method (Robinson 1996, Shapiro 2003) is an important method for solving such stochastic optimization problems. The basic idea of the method is to approximate the mean-value function $F(x)$ in (3) by averaging sample response functions

$$F(x) \approx \bar{f}^N(x) := \frac{1}{N}\sum_{i=1}^{N} f(x,\omega_i), \tag{4}$$

where N is an integer representing the number of samples. (The explicit value of the underlying function $F(x)$ can be determined by letting the number of samples $N\to\infty$, but such computation is typically impractical.) By fixing a sequence of i.i.d. (independent identically distributed) random samples ω_i, $i = 1, 2, \ldots, N$, a variety of deterministic algorithms can be applied to solve the averaged sample-path problem

$$\min_{x\in\mathbb{R}^n} \bar{f}^N(x), \tag{5}$$

which serves as a substitute for (3). The solution $x^{*,N}$ to the problem (5) is then treated as an approximation of x^*, the solution of (3) and $x^{*,N}$ converges to x^* under appropriate conditions (Robinson 1996).

Deng and Ferris (2007) propose a *Variable-Number Sample-Path* (VNSP) scheme, an extension of sample-path optimization. The classical sample-path method is criticized for its excessive simulation evaluations: in order to obtain a solution point $x^{*,N}$, one has to solve an individual optimization problem (5) and at each iterate x_k of the algorithm, $\bar{f}^N(x_k)$ is required (with N typically large). The VNSP scheme is designed to generate different numbers of sample paths (N) at each iteration. Denoting N_k as the number of sample paths at iteration k, Bayesian techniques are applied to establish satisfactory

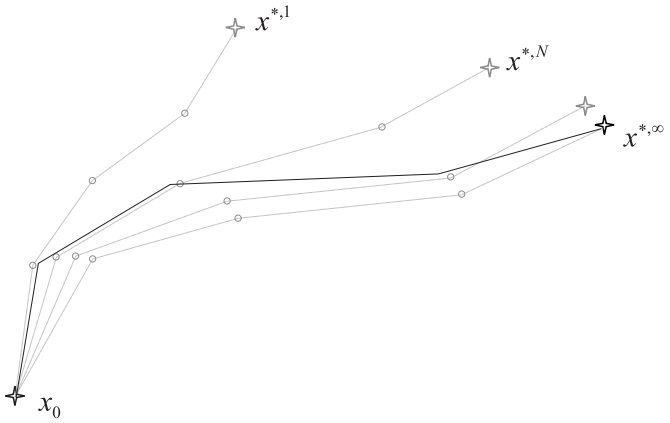

Figure 3. Illustration of variable-number sample-path optimization

criteria for N_k, which accordingly ensure the accuracy of the approximation of $\bar{f}^N(x)$ to $F(x)$. The numbers $\{N_k\}$ form a nondecreasing sequence, with possible convergence to infinity. Figure 3 provides an illustration of the approach. The algorithm generates its iterates across different averaged sample functions. At iteration k, it first computes a satisfactory N_k which guarantees a certain level of accuracy. Then, a single optimization step is taken for problem (5) with $N = N_k$. The algorithm has a globally convergent solution x^{*,N_∞}, where $N_\infty := \lim_{k\to\infty} N_k$, and the solution is proven to match the solution $x^{*,\infty} = x^*$ (Deng and Ferris 2007).

3.2. The extended UOBYQA algorithm

The VNSP scheme is implemented within the UOBYQA algorithm (Powell 2002). UOBYQA is a derivative-free method, thus is a good fit for the objective function derived from the antenna simulation model. The general structure of UOBYQA follows a *model-based approach* (Conn and Toint 1996), which constructs a chain of local quadratic models to approximate the objective function within certain trust regions (Nocedal and Wright 2006).

Starting the algorithm requires an initial point x_0 and an initial trust region radius Δ_0. At each iteration k, the correct sample path number N_k is determined by the Bayesian VNSP scheme of section 3.3, resulting in an averaged sample-path function $\bar{f}^{N_k}$ (an approximation to $\bar{f}^\infty = F(x)$ in (4)). The derivative estimate of $\bar{f}^{N_k}$ is contained in a quadratic model

$$Q_k^{N_k}(x_k + s) = c_k^{N_k} + \left(g_k^{N_k}\right)^T s + \frac{1}{2} s^T G_k^{N_k} s, \tag{6}$$

which is constructed by interpolating a set of well-positioned points $\mathcal{I} = \{y^1, y^2, \ldots, y^L\}$. To ensure a unique quadratic interpolator, the number of points in $\mathcal{I}$ should satisfy $L = \frac{1}{2}(n+1)(n+2)$. Note that deriving the model does not require evaluations of the gradient or the Hessian.

As in a classical trust region method, a new promising point is determined from a subproblem:

$$\min_{s\in\mathbb{R}^n} Q_k^{N_k}(x_k+s), \quad \text{subject to } \|s\| \le \Delta_k. \tag{7}$$

The new solution s^{*,N_k} is accepted (or not) by evaluating the 'degree of agreement' between $\bar{f}^{N_k}$ and $Q_k^{N_k}$:

$$\rho_k^{N_k} = \frac{\bar{f}^{N_k}(x_k) - \bar{f}^{N_k}(x_k+s^{*,N_k})}{Q_k^{N_k}(x_k) - Q_k^{N_k}(x_k+s^{*,N_k})}. \tag{8}$$

If the ratio $\rho_k^{N_k}$ is large enough, the point x_k+s^{*,N_k} is accepted into the set $\mathcal{I}$, otherwise, the geometry of $\mathcal{I}$ should be improved when necessary: details can be found in Deng and Ferris (2007). The trust region radius is then updated following standard trust region rules. Whenever a new point x^+ enters (the point x^+ may be the solution point x_k+s^{*,N_k} or a replacement point to improve the geometry), the best point in $\mathcal{I}$ must be determined.

We now present the outline of the extended UOBYQA algorithm, implementing the VNSP scheme.

Algorithm 1 *Choose a starting point x_0 and an initial trust region radius Δ_0.*

(i) Generate initial trial points in the interpolation set $\mathcal{I}$. Determine the first iterate $x_1 \in \mathcal{I}$ as the best point in $\mathcal{I}$.

(ii) For iterations $k = 1, 2, \ldots$

- *(a) Determine N_k via the VNSP scheme in section 3.3.*
- *(b) Construct a quadratic model $Q_k^{N_k}$ which interpolates points in $\mathcal{I}$.*
- *(c) Solve the trust region subproblem (7). Evaluate $\bar{f}^{N_k}$ at the new point x_k+s^{*,N_k} and compute the agreement ratio $\rho_k^{N_k}$.*
- *(d) Test whether the point is acceptable in the set $\mathcal{I}$ and update the trust region radius Δ_k.*
- *(e) Check whether any of the termination criteria are satisfied, otherwise repeat the loop.*

(iii) Evaluate and return the final solution point.

3.3. The Bayesian VNSP scheme

The goal of the VNSP scheme is to determine the suitable sample path number N_k to be applied at iteration k, such that the accuracy of the algorithm is maintained. While increasing the number N_k can potentially reduce approximation bias, N_k should be kept as small as possible to save computational effort.

The VNSP scheme adopts a strategy that sequentially allocates computational resources: first evaluate and check a satisfactory criterion (often termed as the 'sufficient reduction' criterion)

$$Pr\Big(Q_k^{N_k}(x_k) - Q_k^{N_k}(x_k+s^{*,N_k}) \ge \kappa_{\mathrm{mdc}}\|g_k^{\infty}\| \min\left[\frac{\|g_k^{\infty}\|}{\kappa_{\mathrm{Qh}}}, \Delta_k\right]\Big) \ge 1-\alpha_k, \tag{9}$$

where κ_{mdc} takes the value $\frac{1}{2}$, κ_{Qh} is a large value upper-bounding the norm of the Hessian matrix, and α_k represents the significance level. If the criterion (9) is rejected, increase N_k to improve the accuracy. Typically, N_k is updated by

$$N_k := \beta N_k.$$

The difficulty of validating (9) lies in that the probability value is taken over the sample-path space and the explicit form of Q_k^∞ is unknown. To cope with these problems, the VNSP scheme uses Bayesian probability to approximate the real probability in (9). More specifically, the Bayesian probability is computed using estimated Bayesian posterior distributions for the parameters (g_k^∞, G_k^∞) of the model Q_k^∞: see details in Deng and Ferris (2007).

We summarize the outline of the Bayesian VNSP scheme as follows.

Algorithm 2 (The VNSP Scheme) *At the kth iteration of the algorithm, start with* $N_k = N_{k-1}$. *Loop:*

(i) Evaluate N_k *replications at each point* y^j *in the interpolation set* $\mathcal{I}$ *to construct the data for the Bayesian estimation.*

(ii) Construct the quadratic model $Q_k^{N_k}$ *and solve the subproblem for* $x_k + s^{*,N_k}$.

(iii) Derive the Bayesian posterior distributions for the parameters of Q_k^∞, *and estimate the probability of 'sufficient reduction' in criterion (9).*

(iv) If the probability value is greater than $1 - \alpha_k$, *then stop; otherwise increase* N_k, *and repeat the loop.*

4. Results

4.1. Application of the VNSP optimization

In this section, we apply the new algorithm to optimize an antenna to yield robust performance against uncertainties in tissue parameters.

As a general setting for the algorithm, we set the initial number of samples $N_0 = 3$, which was used to estimate the initial sample mean and sample covariance matrix, and set a predefined sequence in (9):

$$\alpha_k = 0.1 \times (0.98)^k. \tag{10}$$

This sequence satisfies the assumptions required in the convergence theory (Deng and Ferris 2007). Other choices (instead of 0.1 and 0.98) are clearly possible, but we found these values to work well in this application setting. Future work will determine an automatic scheme to set these values. As our proposed method is a local optimization method, the starting point can be significant. The starting point was chosen to be $x_0 =$ (9.00 2.00 20.00 0.15 0.15 16.00), which are the design variables proposed by Yang et al (2006). We limited the maximum number of function evaluations to 2000, therefore, it took roughly 6 h for the entire optimization process. We chose the initial trust region

Table 3. Optimal design search using the new algorithm.

Iteration k	N_k	FN	x_k	$\bar{f}^{N_k}(x_k)$	Δ_k
1	3	3	(9.00 2.00 20.00 0.15 0.15 16.00)	-0.320344	1
51	3	243	(9.81 1.56 19.63 0.41 0.13 16.05)	-0.391705	0.1
52	9	420	(9.69 1.62 19.63 0.41 0.13 16.12)	-0.402081	0.1
53	9	429	(9.69 1.62 19.63 0.41 0.13 16.12)	-0.402081	0.1
54	12	525	(9.68 1.58 19.55 0.42 0.12 16.09)	-0.402388	0.1
74	12	753	(9.70 1.61 19.56 0.42 0.12 16.09)	-0.405788	0.01
75	16	881	(9.69 1.61 19.56 0.42 0.12 16.11)	-0.404821	0.01
76	22	1071	(9.69 1.61 19.56 0.42 0.12 16.11)	-0.404868	0.01
102	22	1621	(9.67 1.62 19.53 0.42 0.12 16.11)	-0.405219	0.01

radius Δ_0 to be 1, which corresponded to a 1 mm local search region centered around the initial design x_0. The normalization values in (2) were $H_1 = 3$, $H_2 = 0.5$, $H_3 = 30$, and $H_4 = 0.5$, which correspond to maximum values expected for each of the individual metrics.

Table 3 presents the results for the robust antenna design search. In iterations 1 to 102, N_k changed from 3 to 22. We recorded the iteration number k when there was a change in N_k. For example, N_k remained at 3 in iterations 1 to 51, and N_k changed to 9 at iteration 52. Since in the first 51 iterations the objective function was $\bar{f}^3$, it was observed that the iterates x_k moved toward the solution $x^{*,3}$ of the averaged sample-path problem (5) with $N = 3$. Table 4 (which took a large amount of time to compute) records the corresponding sample-path solutions of the optimization problem (5). For example, $x^{*,3}$ = (9.70 1.57 19.44 0.42 0.11 16.05). As shown in table 4, solutions $x^{*,N}$ have variations, but tend to converge as N increases. The convergence of the solutions $x^{*,N}$, as well as the optimal objective values $\bar{f}(x^{*,N})$, are proven facts in sample-path optimization literature (Robinson 1996). The variation of $x^{*,N}$ also implies that the optimal designs are sensitive to the uncertain input parameters. With the change of N_k, the averaged function $\bar{f}^{N_k}$ might vary. In table 3, we observe that $x_{75} = x_{76}$ = (9.69 1.61 19.56 0.42 0.12 16.11). However, the value of $\bar{f}^{N_{75}}(x_{75})$ is -0.404821, while the value of $\bar{f}^{N_{76}}(x_{76})$ is -0.404868, proving that the algorithm actually worked when the objective function changed due to an increase in N_k.

In the earlier iterations, when noisy effects were small compared to the large change of function values, the basic operation of the method was unchanged, e.g., $N_k = 3$ for k = 1 to 51. As the algorithm proceeded, the demand for accuracy increased, therefore, N_k increased as well as the total number of function evaluations. We observed significant improvement of the solution in iterations 1 to 51, when $N_k = 3$. At the end of the algorithm, we generated a solution x_{102} = (9.67 1.62 19.53 0.42 0.12 16.11) which yielded an objective value -0.405219 very close to that of $x^{*,22}$ = (9.68 1.63 19.53 0.42 0.12 16.10).

Table 4. Averaged sample-path solutions.

N	$x^{*,N}$	$\bar{f}^N(x_k)$
3	(9.70 1.57 19.44 0.42 0.11 16.05)	-0.393864
9	(9.67 1.63 19.52 0.42 0.11 16.10)	-0.402543
12	(9.74 1.63 19.51 0.41 0.12 16.05)	-0.406015
16	(9.67 1.62 19.53 0.42 0.12 16.10)	-0.404980
22	(9.68 1.63 19.53 0.42 0.12 16.10)	-0.405219
100	(9.68 1.63 19.53 0.42 0.12 16.11)	-0.403319

We did save significant amounts of computation compared to the standard sample-path method. In a standard sample-path method, assuming that there are around 102 iterations in the algorithm, we need $(102 + 28) \times 22 \approx 2860$ function evaluations for the solution $x^{*,N=22}$, where 28 points are used to construct the initial quadratic model, compared to the 1621 that our method used. The optimal objective value did yield a 26.5% improvement over the initial design with respect to the mean function $\bar{f}^{N=22}$.

4.2. Discussion

While comparison of the compound objective function shows that the optimization procedure helped yield an improved design $x^* = (9.67\ 1.62\ 19.53\ 0.42\ 0.12\ 16.11)$, it is important to confirm that improved performance was achieved in terms of the individual metrics. The goal of the optimization process was twofold: (a) improve robustness of the design so that each individual metric is less sensitive to variations in tissue dielectric parameters among individuals and (b) to improve the values of each of the individual metrics. Figure 4 shows the distribution for each of the individual metrics of the optimal design and the design in Yang et al (2006) for a common random sample of 100 different values for the dielectric properties within the ±10% specified range. Also included are the distributions of design presented in Yang et al (2006).

The antenna presented by Yang et al (2006) has the following objective metrics: lesion radius = 1.92 cm, axial ratio = 0.42, S_{11} = -15.9 dB and probe radius = 0.17 cm. In comparison, the optimal design presented in this work has objective metrics: lesion radius = 2.03 cm, axial ratio = 0.48, S_{11} = -17.8 dB and probe radius = 0.20 cm. Table 6 provides the mean and standard deviation for each of the individual metrics.

These results indicate the Bayesian VNSP algorithm yields a design which has improved values for the compound objective and each of the individual objective metrics when compared to the original design of the sleeve antenna, except for probe radius. In particular, the variation in the axial ratio and reflection coefficient of the optimal design are 24% and 90%, respectively, lower than the original design. Although the average value of the lesion radius of the optimal design is larger than that of the original design, there is a 15% increase in standard deviation. If this is an potential issue, we could augment our objective function to incorporate this feature; for example, by introducing an additional term that limits the standard deviation. The probe radius is a function

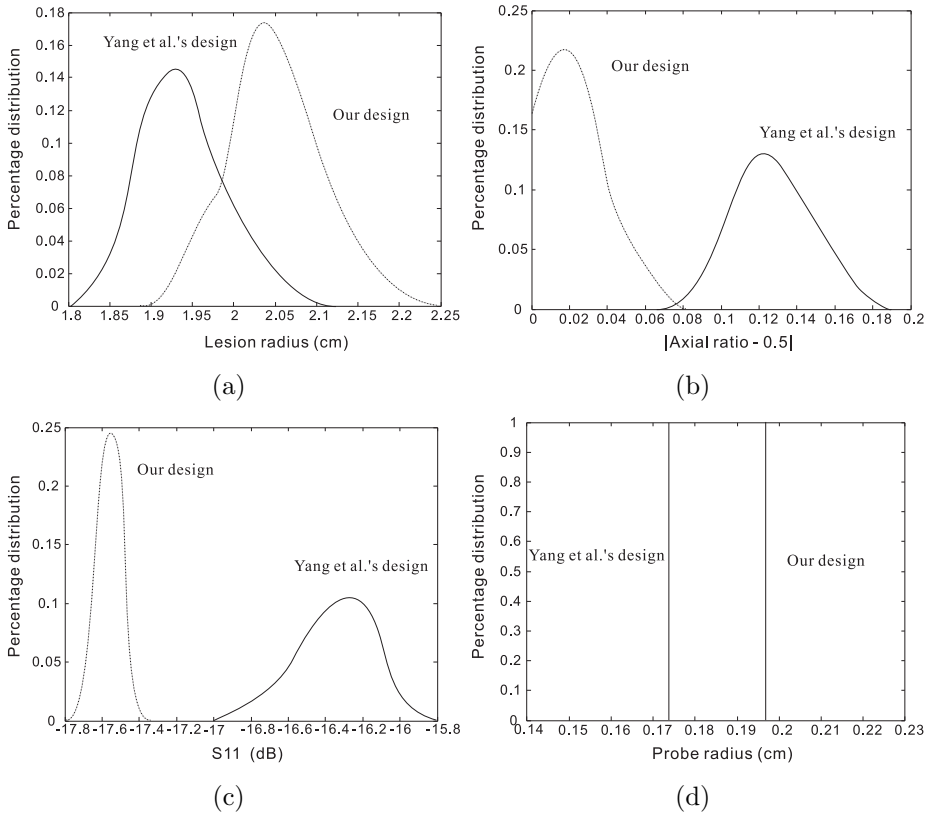

Figure 4. Variations of individual objective metrics (frequency plot). (a) Lesion radius, (b) |Axial ratio - 0.5|, (c) S_{11}, (d) Probe radius

Table 5. Comparison of dimensions of the original and optimized antennas.

Parameter	Design by Yang et al.	Our optimal design
Length of dipole tip	9.00 mm	9.67 mm
Slot size	2.00 mm	1.62 mm
Sleeve position	20.00 mm	19.53 mm
Thickness of Teflon coating	0.15 mm	0.42 mm
Thickness of Teflon isolation layer	0.15 mm	0.12 mm
Length of sleeve	16.00 mm	16.11 mm

of the physical dimensions of the antenna and is thus independent of any variations in tissue properties, which explains its variance of 0 in table 6.

Figure 5 shows $Q(\boldsymbol{r})$ heating profiles of Yang et al.'s design compared to the optimal design presented here when simulating using the average values for dielectric parameters. The optimal design not only creates a larger lesion, but also does better in constraining the lesion to the distal end of the antenna. The antenna designed in Yang et al (2006) has a $Q(\boldsymbol{r})$ profile with a 'tail' along the axis of the antenna, as is clear from figure 5(a).

Table 6. Comparison of the objective metrics of the original and optimized antennas.

	Design by Yang et al.		Our optimal design	
	Mean	Std	Mean	Std
Lesion radius	1.9190	0.0628	2.0313	0.0727
|Axial ratio - 0.5|	0.0785	0.0311	0.0239	0.0237
S_{11}	-15.89	0.2751	-17.75	0.0268
Probe radius	0.1730	0	0.1970	0

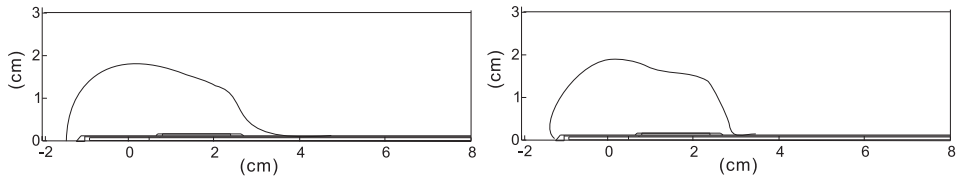

(a) (b)

Figure 5. Comparing simulated $Q(\boldsymbol{r})$ profiles using the average dielectric properties (43.03,1.69). (a) antenna design presented by Yang et al. (b) optimal design derived by our algorithm

Note that for both antennas, the actual longitudinal extent of the lesion after taking into account thermal conductivity is likely to be even larger, thereby potentially destroying large amounts of healthy tissue. While it is plausible that the optimal design may also exhibit a 'tail' in the lesion after considering effects of thermal conductivity, it is likely to be much smaller since the amount of electromagnetic power deposited along the axis of the coaxial cable is much smaller.

The probe radius of the optimal design is slightly larger than that in Yang et al (2006). However, both designs are well within the range of probes typically used in percutaneous applications. If a smaller probe radius is desirable, the weight associated with this metric (w_4) may be emphasized. There is also a slight improvement in reflection coefficient, although the difference in the actual amount of power reflected is negligible.

The optimized antenna has a $Q(\boldsymbol{r})$ profile with axial ratio closer to 0.5 (which is the axial ratio a perfectly spherical lesion would yield) than Yang et al.'s design. Notice that the shape of the $Q(\boldsymbol{r})$ profile is not perfectly spherical. This is because the metric employed only considers the extents of the lesion in the longitudinal and radial directions. An improved metric that analyzes the shape of the lesion along its entire boundary may help yield even better designs.

5. Conclusions

We have optimized the design of a floating sleeve antenna for microwave ablation of hepatic tumours using finite element models and the Bayesian VNSP algorithm. This was done by identifying desirable features for a coaxial antenna for this application and

formulating a mathematical optimization problem to select the dimensions of the floating sleeve antenna that optimize these features. We accounted for the natural variation in physical properties of liver tumours/tissue among individuals by incorporating a stochastic component into the optimization problem and we used a Bayesian VNSP method to solve the optimization problem which decreased the total optimization time significantly.

We achieved a substantial improvement in the variation in two of the three objective metrics (axial ratio and S_{11}) as a function of dielectric properties of the tissue, although variation in lesion radius slightly increased. Mean values of all the objective metrics of the optimum design except the probe radius were superior to the original design of the sleeve antenna.

While our method yields an improved design, several aspects of the procedure may be enhanced to yield even better performance. The metric we have used for assessing lesion shape only utilizes knowledge of the maximal extents in the radial and longitudinal directions. An improved metric would analyze features along the entire lesion boundary. In order to ease computational burden, we have neglected effects of thermal conductivity. These effects may be included to improve the accuracy of the finite element model. Lastly, availability of more measurements of dielectric properties of human liver tumours would allow for better modelling in the variation of these properties.

Acknowledgments

This material is based on research partially supported by NSF grants DMI-0521953, DMS-0427689 and IIS-0511905, AFOSR grant FA9550-04-1-0192, and NIH grant DK58839.

References

Bertram J M, Yang D, Converse M C, Webster J G and Mahvi D 2006 A review of coaxial-based interstitial antennas for hepatic microwave ablation *Crit. Rev. Biomed. Eng.* **34**, 187–213.

Conn A R and Toint P L 1996 An algorithm using quadratic interpolation for unconstrained derivative free optimization *Nonlinear Optimization and Applications* (New York: Plenum Press) ed G D Pillo and F Giannessi pp. 27–47

Deng G and Ferris M C 2007 Variable-number sample-path optimization To appear in Math. Program., Series B.

Duck F A 1990 *Physical Properties of Tissue: A Comprehensive Reference Book* Academic Press: Harcourt Brace Jovanovich.

Gabriel S, Lau R W and Gabriel C 1996 The dielectric properties of biological tissues: III. parametric models for the dielectric spectrum of tissues *Phys. Med. Biol.* **41**, 2271–2293.

Gürkan G, Özge A Y and Robinson S M 1996 Sample-path solution of stochastic variational inequalities, with applications to option pricing *Proc. 1996 Winter Simulation Conf.* 337–344.

Gürkan G, Özge A Y and Robinson S M 1999 Solving stochastic optimization problems with stochastic constraints: An application in network design *Proc. 1999 Winter Simulation Conf.* 471–478.

Iskander M F and Tumeh A M 1989 Design optimization of interstitial antennas *IEEE Trans. Biomed. Eng.* **36**(2), 238–246.

Kleywegt A J, Shapiro A and Homem–de–Mello T 2001 The sample average approximation method for stochastic discrete optimization *SIAM J. Optimization* **12**, 479–502.

Nocedal J and Wright S J 2006 *Numerical Optimization* second edn Springer New York.

Plambeck E L, Fu B R, Robinson S M and Suri R 1993 Throughput optimization in tandem production lines via nonsmooth programming *Proc. 1993 Summer Computer Simulation Conf.* 70–75.

Plambeck E L, Fu B R, Robinson S M and Suri R 1996 Sample-path optimization of convex stochastic performance functions *Math. Program.* **75**, 137–176.

Powell M J D 2002 UOBYQA: Unconstrained optimization by quadratic approximation *Math. Program.* **92**, 555–582.

Robinson S M 1996 Analysis of sample-path optimization *Math. Oper. Res.* **21**, 513–528.

Shapiro A 2003 Monte Carlo sampling approach to stochastic programming *ESAIM:Proc.* **13**, 65–73.

Stauffer P R, Rossetto F, Prakash M, Neuman D G and Lee T 2003 Phantom and animal tissues for modeling the electrical properties of human liver *Int. J. Hyperthermia* **19**(1), 89–101.

Yang D, Bertram J M, Converse M C, O'Rourke A P, Webster J G, Hagness S C, Will J A and Mahvi D M 2006 A floating sleeve antenna yields localized hepatic microwave ablation *IEEE Trans. Biomed. Eng.* **53**(3), 533–537.